BIOCHEMISTRY
including biophysical chemistry & molecular biology

Article

pubs.acs.org/biochemistry

Role of Aromatic Interactions in Amyloid Formation by Islet Amyloid Polypeptide

Ling-Hsien Tu[†] and Daniel P. Raleigh*[,†,‡]

[†]Department of Chemistry, Stony Brook University, Stony Brook, New York 11794-3400, United States

[‡]Graduate Program in Biochemistry and Structural Biology, Stony Brook University, Stony Brook, New York 11794-3400, United States

Supporting Information

ABSTRACT: Aromatic−aromatic and aromatic−hydrophobic interactions have been proposed to play a role in amyloid formation by a range of polypeptides, including islet amyloid polypeptide (IAPP or amylin). IAPP is responsible for amyloid formation in patients with type 2 diabetes. The polypeptide is 37 residues long and contains three aromatic residues, Phe-15, Phe-23, and Tyr-37. The ability of all single aromatic to leucine mutants, all double aromatic to leucine mutants, and the triple leucine mutant to form amyloid were examined. Amyloid formation was almost twice as rapid for the F15L mutant as for the wild type but was almost 3-fold slower for the Y37L mutant and almost 2-fold slower for the F23L mutant. Amyloid fibrils formed from each of the single mutants were effective at seeding amyloid formation by wild-type IAPP, implying that the fibril structures are similar. The F15L/F23L double mutant has a larger effect than the F15L/Y37L double mutant on the rate of amyloid formation, even though a Y37L substitution has more drastic consequences in the wild-type background than does the F23L mutation, suggesting nonadditive effects between the different sites. The triple leucine mutant and the F23L/Y37L double mutant are the slowest to form amyloid. F15 has been proposed to make important contacts early in the aggregation pathway, but the data for the F15L mutant indicate that they are not optimal. A set of variants containing natural and unnatural amino acids at position 15, which were designed to conserve hydrophobicity, but alter α-helix and β-sheet propensity, were analyzed to determine the properties of this position that control the rate of amyloid formation. There is no correlation between β-sheet propensity at this position and the rate of amyloid formation, but there is a correlation with α-helical propensity.

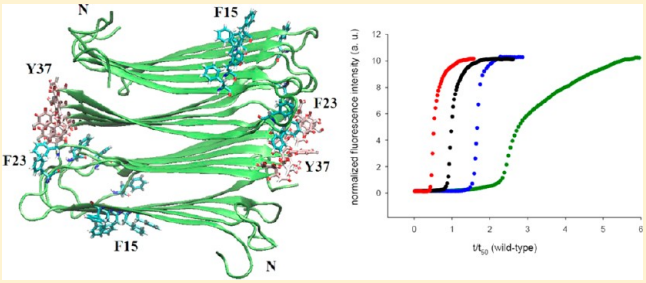

Amyloid formation plays a role in a range of human diseases, and a much larger universe of proteins can be induced to form amyloid in vitro.[1−4] Amyloid formation also plays a functional, beneficial role in certain cases, and amyloid-like structures have been proposed as biomaterials.[5] The proteins and peptides that form amyloid can be divided into two broad classes: those that are largely unstructured, "intrinsically disordered", in their monomeric state and those that form compact globular structures. Important examples of intrinsically disordered sequences that form amyloid include the Aβ peptide of Alzheimer's disease and islet amyloid polypeptide (IAPP or amylin), the protein responsible for islet amyloid in type 2 diabetes.[6−8] IAPP is an endocrine partner to insulin, is synthesized in the pancreatic β-cells, is stored in the insulin secretory granules, and is released in response to the same stimuli that promote insulin release.[9−11] Amyloid formation by IAPP is believed to contribute to the loss of β-cell mass in type 2 diabetes and to graft failure after islet transplantation.[12−14]

The details of amyloid formation are still not well understood, especially for those proteins that are intrinsically disordered in their monomeric states. Aromatic−aromatic interactions have been proposed to play an important role in amyloid formation, particularly for IAPP.[15−17] IAPP contains three aromatic residues, F15, F23, and Y37 (Figure 1), and a triple aromatic to leucine mutant forms amyloid at a significantly reduced rate compared to that of the wild type;[16] however, the effects of single site substitutions or double mutations have not been examined. Phe to Tyr FRET studies suggest that aromatic residues may make contacts during the early stages of amyloid formation.[18] However, experiments with variants that contain the fluorescent Tyr analogue 4-cyanophenylalanine argue that the aromatic side chains remain solvated during the lag phase and suggest that aromatic−aromatic interactions involving Y37 do not develop during the lag phase.[19] Thus, the role of the aromatic residues in amyloid formation by IAPP is not clear. In fact, the details of the early stages of IAPP amyloid formation are not well understood. This is a topic of current interest because intermediates along the pathway of amyloid formation may

Received: October 18, 2012
Revised: December 19, 2012
Published: December 20, 2012

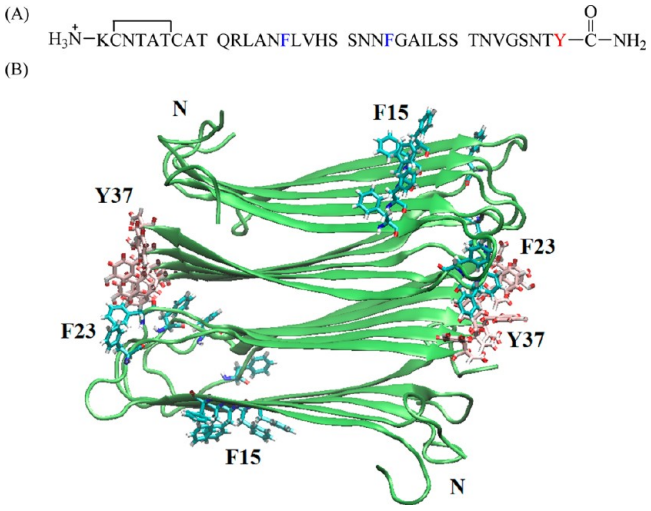

Figure 1. (A) Primary sequence of human IAPP. IAPP contains a disulfide bridge between residues 2 and 7. The C-terminus is amidated, and the N-terminus is free. The aromatic residues are colored blue (F15 and F23) and red (Y37). (B) Diagram of the solid-state nuclear magnetic resonance-derived model of IAPP protofibrils.[26] The aromatic residues and the N-terminus are labeled. F23 (blue) and Y37 (red) are colored differently as an aid to the eye.

be the most toxic entities and could be targets for inhibitor design.[7,20,21] The role of F15 is particularly interesting because this position is believed to make contacts important for the initial oligomerization.[22] Here we examine a comprehensive set of aromatic to leucine mutants as well as a set of F15 variants containing natural and unnatural amino acids that preserve hydrophobicity but alter secondary structure propensity to deduce the role aromatic residues play in amyloid formation by IAPP.

MATERIALS AND METHODS

Peptide Synthesis and Purification. Peptides were synthesized on a 0.25 mmol scale using a CEM microwave peptide synthesizer and 9-fluorylmethoxycarbonyl (Fmoc) chemistry. Fmoc-protected pseudoproline dipeptide derivatives were incorporated at positions 9 and 10, 19 and 20, and 27 and 28 to facilitate the synthesis.[23] Solvents were ACS-grade. All other reagents were purchased from Advanced Chemtech, PE Biosystems, Sigma, and Fisher Scientific. 5-(4′-Fmoc-amino-methyl-3′,5-dimethoxyphenol)valeric acid (PAL-PEG) resin was used to form an amidated C-terminus. Standard Fmoc reaction cycles were used. The first residue attached to the resin, β-branched residues, Arg, and all pseudoproline dipeptide derivatives were doubly coupled. The peptide was cleaved from the resin through the use of standard trifluoroacetic acid (TFA) methods. Crude peptides were partially dissolved in 20% acetic acid (v/v), frozen in liquid nitrogen, and lyophilized to increase their solubility. The dry peptide was dissolved in dimethyl sulfoxide (DMSO) at room temperature to promote the formation of the disulfide bond.[24,25] The peptides were purified by reverse-phase high-performance liquid chromatography (HPLC) using a Vydac C18 preparative column (10 mm × 250 mm). A two-buffer gradient was used: buffer A consisting of 100% H_2O and 0.045% HCl (v/v) and buffer B consisting of 80% acetonitrile, 20% H_2O, and 0.045% HCl. HCl was used as the counterion instead of TFA to reduce the residual amount of TFA because TFA can influence amyloid formation. Analytical HPLC was used to check the purity of peptides before each experiment. Peptides were analyzed by mass spectrometry using a Bruker MALDI-TOF MS instrument to confirm the molecular weight: wild-type IAPP, expected 3903.3, observed 3902.1; F15-IAPP, expected 3871.3, observed 3872.0; F23-IAPP, expected 3871.3, observed 3871.3; Y37-IAPP, expected 3855.4, observed 3853.8; F15L/F23L-IAPP, expected 3835.3, observed 3834.0; F15L/Y37L-IAPP, expected 3821.3, observed 3819.8; F23L/Y37L-IAPP, expected 3821.3, observed 3820.0; 3XL-IAPP, expected 3787.2, observed 3785.1; F15I-IAPP, expected 3871.3, observed 3871.5; F15NLe-IAPP, expected 3871.3, observed 3872.1; F15TLe-IAPP, expected 3871.3, observed 3872.0.

Sample Preparation. A 1.6 mM peptide solution was prepared in 100% hexafluoro-2-propanol (HFIP) and stored at −20 °C. For kinetic experiments, 17 μL of the filtered stock solution was diluted into 20 mM Tris-HCl buffer to give a final IAPP concentration of 16 μM in 2% HFIP. This condition was chosen to facilitate comparison with previously published studies. For the seeding assays, preformed wild-type IAPP and single-mutant fibrils were produced by diluting a 1.6 mM stock solution of peptide in HFIP into 20 mM Tris-HCl buffer containing thioflavin T at pH 7.4 for a final IAPP concentration of 16 μM in 2% HFIP. The solution was incubated, and thioflavin T fluorescence was monitored to ensure fibril formation had occurred. Seeds were used within 12 h to ensure reproducibility.

Thioflavin T Fluorescence Assays. Fluorescence experiments were performed on an Applied Phototechnology fluorescence spectrophotometer using an excitation wavelength of 450 nm and an emission wavelength of 485 nm. The excitation and emission slits were set at 6 nm, and a 1.0 cm cuvette was used. Solutions were prepared by diluting the filtered stock solution using a 0.45 μm GHP Acrodisc 13 syringe filter into Tris-HCl buffer and thioflavin T solution immediately before the measurement. The final concentrations were 16 μM peptide and 32 μM thioflavin T in 2% HFIP and 20 mM Tris-HCl (pH 7.4) for all experiments. All solutions were stirred during the fluorescence experiments to maintain homogeneity. Stirring is known to accelerate IAPP amyloid formation. For the seeding assays, 1.6 mM peptide stock solutions in HFIP were diluted into the seeded buffer solution to give final concentrations of 16 μM peptide, 32 μM thioflavin T, 1.6 μM seed (in monomer units), and 2% HFIP in 20 mM Tris-HCl (pH 7.4). For kinetic experiments without HFIP, solutions were prepared by adding 20 mM Tris-HCl buffer (pH 7.4) containing thioflavin T to lyophilized dry peptides for a final peptide concentration of 16 μM. These studies were conducted using a Beckman Coulter DTX880 plate reader without stirring.

Circular Dichroism (CD) Experiments. CD experiments were performed at 25 °C using an Applied Photophysics Chirascan CD spectrometer. The solutions for the CD experiments were prepared by diluting the filtered stock peptide solutions into 20 mM Tris-HCl buffer (pH 7.4). The final peptide concentration was 16 μM in 2% HFIP. Spectra were recorded from 190 to 260 nm at 1 nm intervals in a quartz cuvette with a 0.1 cm path length at 25 °C. CD experiments used the same stock solutions as the thioflavin T fluorescence measurements. A background spectrum was subtracted from the collected data.

Transmission Electron Microscopy (TEM). TEM was performed at the Life Science Microscopy Center at Stony

Brook University. Samples were aliquots from the same solutions that were used for the fluorescence measurements. Five microliters of the peptide solution was placed on a carbon-coated Formvar 300 mesh copper grid for 1 min and then negatively stained with saturated uranyl acetate for 1 min.

RESULTS AND DISCUSSION

Analysis of Amyloid Formation by Aromatic to Leu Variants. The sequence of IAPP and the solid-state nuclear magnetic resonance (NMR)-derived model of IAPP amyloid protofibrils[26] are shown in Figure 1. The molecule contains a disulfide bond between Cys-2 and Cys-7 and has an amidated C-terminus. F15 and Y37 are conserved among all known IAPP sequences; F23 is not, but it is substituted with only leucine (Supporting Information). A set of seven aromatic to leucine variants were prepared: all three single mutants, the complete set of double mutants, and the triple mutant. Leu was used because it is the closest natural nonaromatic substitution for Tyr and Phe in terms of size and hydrophobicity. An additional set of variants was prepared to examine the role of Phe-15 in detail.

The rate of amyloid formation was measured using fluorescence-detected thioflavin T binding assays. Thioflavin is a small dye whose quantum yield is enhanced when it binds to amyloid fibrils.[27] The molecule is believed to bind to grooves on the surface of the amyloid fibrils. Thioflavin T assays reliably report on IAPP amyloid formation kinetics, and the compound does not alter the aggregation kinetics under the conditions used here. Amyloid formation by IAPP follows a sigmoidal time course in which no detectable amyloid fibrils are formed during the lag phase. The lag phase is followed by a growth phase during which fibrils develop and elongate, eventually leading to a steady state where fibrils are in equilibrium with soluble protein. Thioflavin T curves for the wild type and single mutants are displayed in Figure 2A, and the data for the double and triple mutants are shown in Figure 2B. Amyloid formation by wild-type IAPP is rapid under the conditions of these experiments (2% HFIP, 20 mM Tris-HCl, pH 7.4, and constant stirring). IAPP amyloid formation has been widely studied by dilution from HFIP, and we chose this protocol to facilitate comparison to earlier studies. Additional studies, described below, were performed without HFIP.

The kinetic analysis reveals a number of interesting features. All of the mutants, with the exception of F15L, show a decreased rate of amyloid formation and an increased lag time. In contrast, replacement of F15 accelerates amyloid formation, decreasing the lag time by a factor of almost 2. F15 has been proposed to be involved in the early steps of amyloid formation, but the data show that the Phe-15 is not the optimal residue at this site in terms of amyloid formation. The role of F15 is considered in more detail below. The other single mutants form amyloid more slowly with the most pronounced effect observed for the Y37 mutant, which has a lag time that is a factor of 3 longer than that of wild-type IAPP. The lag time for F23L is almost 2-fold longer than that of the wild type. The F15L/Y37L double mutant forms amyloid more rapidly than the Y37L single mutant, but more slowly than the wild type, indicating that the acceleration caused by the F15 substitution partially compensates for the slowing caused by the Y37L replacement. The other mutants are much slower in forming amyloid than wild-type IAPP. F15L/F23L-IAPP is 4-fold slower, while F23L/Y37L-IAPP and 3XL-IAPP are ~7.5-fold slower. The lag times and t_{50} values for all of the mutants are

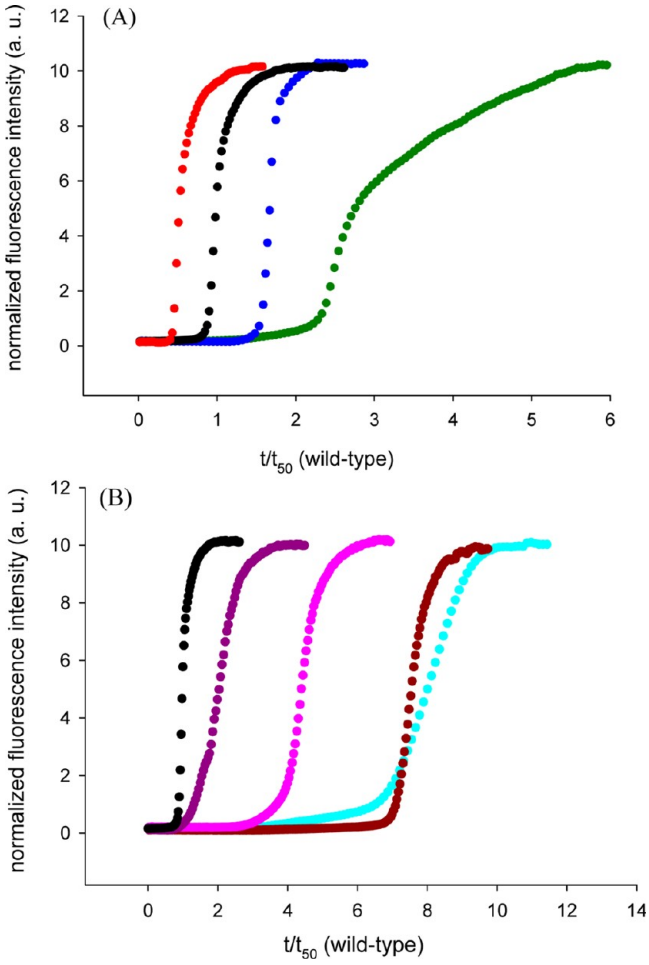

Figure 2. Substitution of the aromatic residues in IAPP alters the kinetics of amyloid formation. Thioflavin T fluorescence-monitored kinetic experiments. (A) Single mutants compared to the wild type: black for wild-type IAPP, red for F15L-IAPP, blue for F23L-IAPP, and green for Y37L-IAPP. (B) Multiple mutants compared to the wild type: black, wild-type IAPP; purple, F15LY37L-IAPP; pink, F15LF23L-IAPP; brown, F23LY37L-IAPP; and light blue, 3XL-IAPP. All experiments were conducted in 20 mM Tris buffer (pH 7.4) and 2% HFIP with constant stirring at 25 °C.

listed in Table 1. T_{50} is the time required to reach half the final intensity in a thioflavin T assay and is commonly used as a quantitative measure of amyloid formation. The differences observed for t_{50} values and the lag times between different peptides are much larger than the experimental uncertainty. For examples, analysis of a set of 25 independent measurements conducted on wild-type IAPP over the course of two years with more than five separate batches of peptide yielded a standard deviation in t_{50} of <20% (Supporting Information). The calculated standard deviations for independent measurements conducted on an individual batch of peptide are even smaller, <10% in all cases and often significantly smaller. TEM images of aliquots removed at the end of each kinetic run confirm the presence of extensive amyloid fibrils (Figure 3 and the Supporting Information). CD confirms the presence of β-sheet structure in all samples (Supporting Information).

The differences in the rates of amyloid formation are unlikely to be due to small variations in concentration from sample to sample, because the lag time for amyloid formation by IAPP has been shown to be largely independent of peptide concentration

dx.doi.org/10.1021/bi3014278 | Biochemistry 2013, 52, 333−342

Table 1. Comparison of Kinetic Parameters for Wild-Type IAPP and Aromatic to Leucine Mutants[a]

peptide	lag time[b] (s)	t_{50}[c] (s)	lag time/wild-type lag time	t_{50}/wild-type t_{50}
wild-type	1310 ± 280[d]	1470 ± 280		
F15L-IAPP	490 ± 50	640 ± 40	0.4 ± 0.1[e]	0.4 ± 0.1
F23L-IAPP	2230 ± 220	2470 ± 220	1.7 ± 0.4	1.7 ± 0.3
Y37L-IAPP	2790 ± 90	4160 ± 100	2.1 ± 0.5	2.8 ± 0.5
F15L/F23L-IAPP	5100 ± 60	5850 ± 30	3.9 ± 0.8	4.0 ± 0.8
F15L/Y37L-IAPP	1790 ± 140	2650 ± 100	1.4 ± 0.3	1.8 ± 0.4
F23L/Y37L-IAPP	9670 ± 150	10600 ± 500	7.4 ± 1.6	7.2 ± 1.4
3XL-IAPP	9210 ± 260	10950 ± 250	7.0 ± 1.5	7.4 ± 1.4

[a]Experiments performed at 25 °C and pH 7.4 in 20 mM Tris-HCl and 2% (v/v) HFIP with constant stirring. [b]The lag time is defined here as the time required to reach 10% of the final fluorescence change in the thioflavin T assays. [c]t_{50} is the time required to reach 50% of the final fluorescence change in the thioflavin T assays. [d]The quoted uncertainty is the standard deviation. [e]The uncertainty was determined by standard propagation of error.

for the conditions (2% HFIP with constant stirring) and concentrations used here.[28] Small changes in pH can affect the rate of amyloid formation by IAPP because the lag time depends on the protonation state of His-18 and the N-terminus;[29] however, all samples were at the same pH to within 0.1 pH unit. Control experiments with wild-type IAPP show that the lag time varies by only 10% between pH 7.2 and 7.6 in the buffer used here (Supporting Information). This variation in pH is much wider than that observed in our experiments, and the effect on the lag time in the control studies is much weaker than the differences in the lag times observed for the different mutants. Variations in the final HFIP concentration can also alter the rate of amyloid formation, but the HFIP concentration was fixed at 2% (v/v).

We also plotted the kinetic data as normalized fluorescence intensity versus normalized time, t/t_{50} (wild-type), to facilitate a comparison of the shape of the kinetic progress curves of the mutants with that of the wild type (Supporting Information). The normalized curves for wild-type IAPP, F15L-IAPP, F23L-IAPP, and F15L/F23L-IAPP are very similar in shape. This is consistent with the mutants and wild-type IAPP having a similar mode of assembly but does not prove that they do. The normalized curve for F15L/Y37L-IAPP shows some differences relative to that of the wild type in the early stage of fibril formation, while the normalized plot for Y37L-IAPP has a slight difference in the growth phase. The F23L/Y37L-IAPP and 3XL-IAPP mutants have the slowest rates of amyloid formation and display the largest differences in normalized progress curves.

The Single Mutants Form Amyloid Fibrils That Are Similar to Wild-Type Fibrils. The TEM and CD studies outlined above suggest that the morphologies of the fibrils formed by wild-type IAPP and the mutants are similar. We investigated the structural similarity between wild-type and mutant fibrils in more detail by conducting seeding experiments. Preformed amyloid fibrils can serve as a template for the addition of monomers, resulting in a bypassing of the lag phase. Seeding is usually much more effective when fibrils are used as seeds for their own monomers.[30,31] We first examined seeding of wild-type IAPP by wild-type fibrils (Figure 4, gray curve). A bypass of the lag phase was observed as expected. We then tested the ability of preformed F15L-IAPP, F23L-IAPP, and Y37L-IAPP amyloid fibrils to seed wild-type IAPP (Figure 4, red, blue, and green curves). The curves perfectly overlap with the curve from the wild-type seeding study, showing that the mutant fibrils seed wild-type IAPP efficiently. This argues that the single-mutant fibrils share significant structural similarity with wild-type fibrils. We also used wild-type fibrils to seed the single mutants (Supporting Information). The mutants can be seeded by wild-type fibrils, but with different seeding efficiencies. The apparent seeding efficiency correlates with the rate of the unseeded reaction in this case.

Nonadditive Effects on Amyloid Formation Are Observed between Different Sites. The effect of some of the double mutations is not equal to the additive effect of the two individual mutations (Figure 5). For a simple protein folding reaction, nonadditive effects can be detected by comparing the effect of mutations on folding rate constants. Independent effects will lead to additive effects on the log of the folding rate or multiplicative effects on the rate constants. Amyloid formation is more complex, involving multiple steps and possible parallel pathways with heterogeneous intermediates; thus, it is not possible to readily relate a simple thioflavin T progress curve to microscopic rate constants. Nonetheless, a semiquantitative comparison can be obtained using valves of t_{50} or the length of the lag phase. We first analyzed the effect caused by a single mutation relative to the wild type by calculating the ratio of the t_{50} of the single mutant to the t_{50} of the wild type. The expected additive effects (stars in Figure 5) are estimated by multiplying the parameters calculated for two single mutations. Assuming independent additive effects, the F15L/F23L double mutant is expected to form amyloid on the same time scale as or even slightly faster than the wild type. However, the value of t_{50} for the F15L/F23L double mutant is 4-fold larger than the wild-type t_{50}. The F15L/Y37L double mutant forms amyloid close to the rate expected if the effect of the F15 mutation and the effect of the Y37 mutation are additive. The F23L/Y37L double mutant has the most significant effect on the rate of amyloid formation (7.2-fold larger than that of the wild type), but the effect is even greater than expected from simple additivity (4.8-fold). To summarize, both the F15L/F23L and F23L/Y37L double mutants form amyloid more slowly than predicted from simple additive effects, with the largest deviation observed for the F15L/F23L double mutant.

Sensitivity of Position 15 to Amyloid Formation. F15L-IAPP is a rare example of a mutation that accelerates amyloid formation. This region of IAPP has been proposed to be involved in the early stages of oligomerization,[22] and it is of interest to determine the properties of this site that impact the rate of amyloid formation. Secondary structure propensity is likely a key feature. Work from several groups suggests that helical intermediates are important in the pathway of IAPP fibrillation.[22,32−37] For example, crystallographic studies of IAPP fused to maltose binding protein showed that the segments corresponding to residues 8−18 and 22−27 are helical in the construct. NMR studies have shown that human and rat IAPP have a tendency to preferentially sample helical ϕ and ψ angles between residues 8 and 22 in the monomeric

dx.doi.org/10.1021/bi3014278 | Biochemistry 2013, 52, 333−342

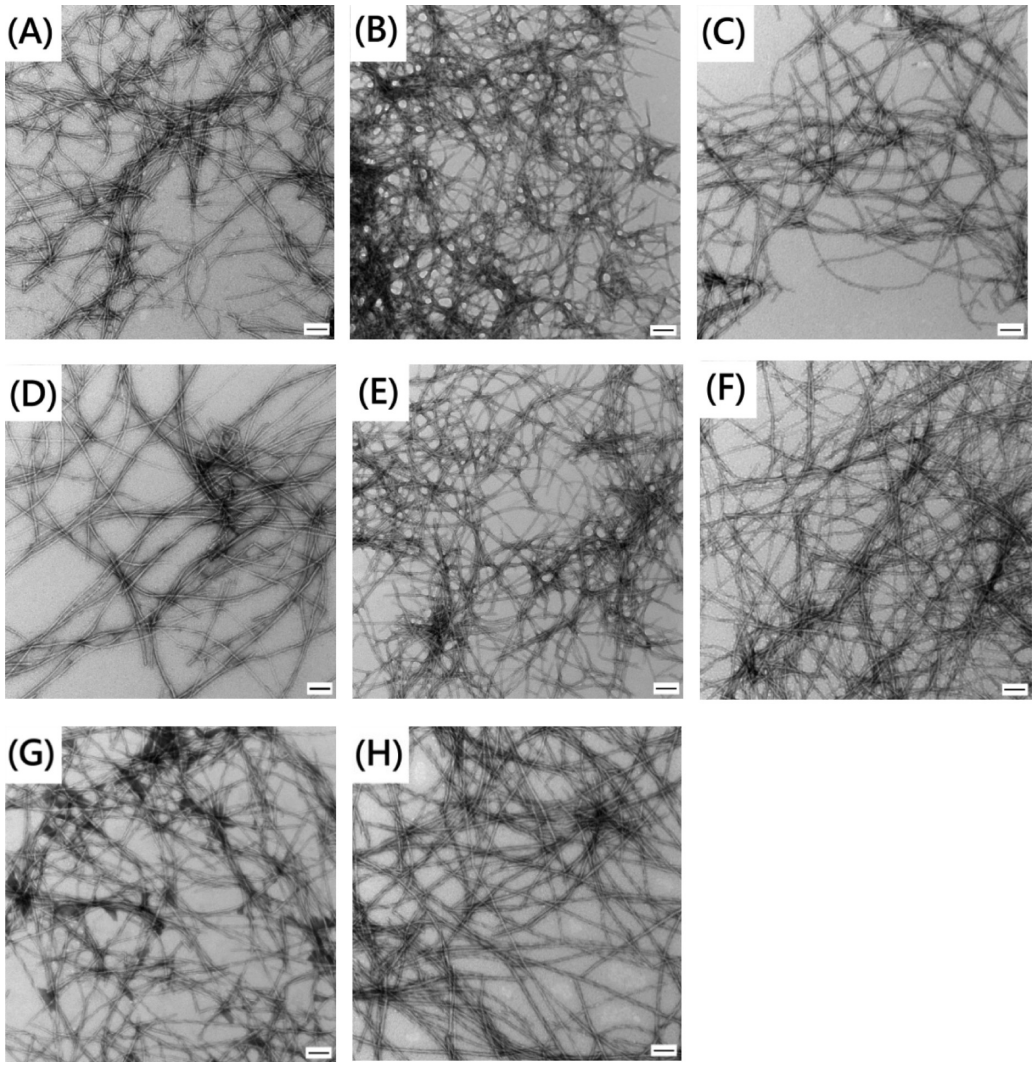

Figure 3. All aromatic mutants form amyloid. TEM images recorded at the end of the kinetic runs depicted in Figure 2: (A) wild-type IAPP, (B) F15L-IAPP, (C) F23L-IAPP, (D) Y37L-IAPP, (E) F15L/F23L-IAPP, (F) F15L/Y37L-IAPP, (G) F23L/Y37L-IAPP, and (H) 3XL-IAPP. The scale bar represents 100 nm.

state.[32] These observations have led to models that postulate that initial oligomerization is driven by the thermodynamic linkage between helix formation and self-association.[22,32,34−37] F15 is within the putative helical region and has been proposed to make important contacts during the early stages of amyloid formation.[22,38]

We prepared a series of variants with isomeric four-carbon side chains at position 15 to probe the factors that control amyloid formation. We compared the effects of Leu, norleucine (four-carbon unbranched side chain), Ile, and *tert*-leucine (*tert*-butyl side chain) on amyloid formation. These amino acids have side chains with similar hydrophobicities,[39] but different α-helix and β-sheet propensities (Figure 6 and the Supporting Information). The substitutions have significantly different effects upon the kinetics of amyloid formation (Figure 6B and the Supporting Information). The F15 to *tert*-leucine variant, (F15TLe-IAPP), which has three methyl groups on the β-carbon, takes much longer to form amyloid than the wild type (Figure 6B, purple), even though TLe has the highest β-sheet propensity.[40−42] The F15I-IAPP mutant (Figure 6C, green curve), with its β-branched side chain, also forms amyloid more slowly than wild-type IAPP, F15L-IAPP, or the F15 to norleucine mutant (F15NLe-IAPP), even though Ile has a higher β-sheet propensity. TEM images confirm that all of the F15 variants form amyloid fibrils and have a morphology similar to that of wild-type fibrils (Figure 7). CD shows that all of these variant fibrils are rich in β-sheet structure (Supporting Information). Seeding experiments were used to further probe the structure of the amyloid fibrils formed by the variants. Each variant was as efficient at seeding amyloid formation by wild-type IAPP as were wild-type seeds (Figure 8), arguing that the structures of the mutant fibrils are similar to wild-type fibrils.

The data show that the rate of amyloid formation does not correlate with β-sheet propensity at this position even though residue 15 is located in a β-strand in all known models of IAPP amyloid fibrils.[26,43] There is a stronger correlation with α-helical propensity. TLe has by far the lowest α-helical propensity,[40,44] and this variant is by far the slowest to form amyloid. Ile has the second lowest helical propensity, and the Ile variant is the second slowest to form amyloid. Phe, the wild-type residue, Leu, and NLe have relatively high α-helical propensities, and these variants form amyloid more rapidly. Earlier work, using truncated variants of IAPP, has shown that

dx.doi.org/10.1021/bi3014278 | *Biochemistry* 2013, 52, 333−342

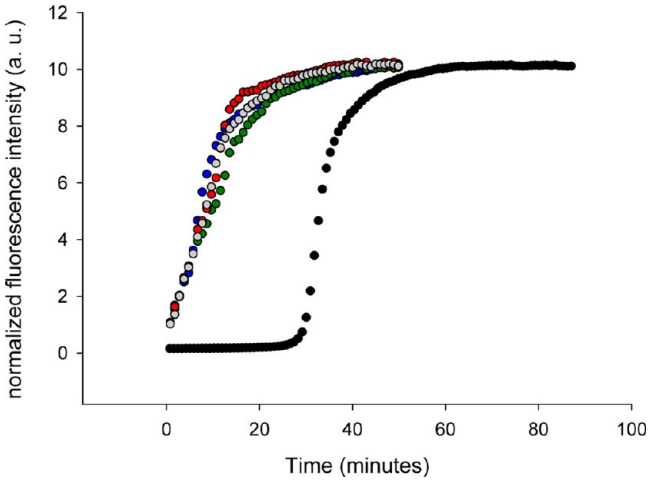

Figure 4. Aromatic mutants effectively seed amyloid formation by wild-type IAPP. Thioflavin T fluorescence-monitored seeding experiments are shown: black for unseeded wild-type IAPP amyloid formation, gray for wild-type IAPP seeded by wild-type IAPP amyloid fibrils, red for wild-type IAPP seeded by F15L-IAPP amyloid fibrils, blue for wild-type IAPP seeded by F23L-IAPP amyloid fibrils, and green for wild-type IAPP seeded by Y37L-IAPP amyloid fibrils.

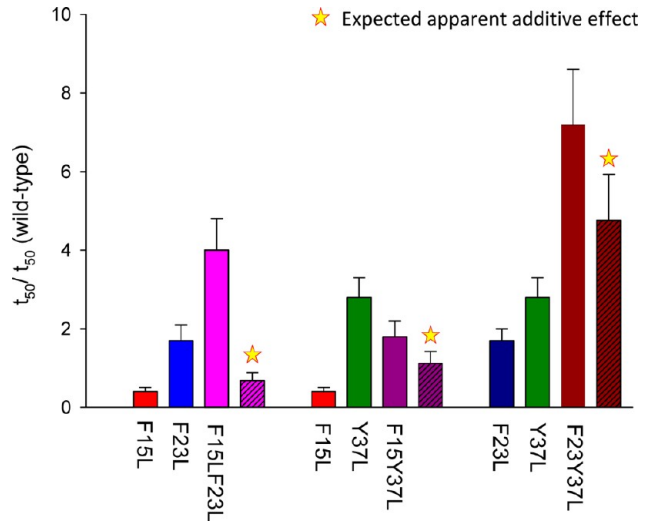

Figure 5. Nonadditive effects of double mutants. The bar graphs show the different effects caused by single mutants and the corresponding double mutants on amyloid formation. Stars denote the expected additive result. The uncertainties represent the standard deviations for experimental data and the propagated uncertainty for calculated values.

replacement of F15 with Ser or Ala increases the rate of amyloid formation.[22] Both of these residues have higher helical propensity than Phe.

The Effect of F15 Substitutions upon Amyloid Formation Is Independent of the Presence of HFIP. HFIP and other fluoridated alcohols accelerate amyloid formation by IAPP, and even low levels of fluoridated alcohol cosolvent can promote helix formation.[28,29] We examined the set of F15 variants in the absence of HFIP to ensure that the results were not biased by the presence of the cosolvent. The lag times for wild-type IAPP and the F15 variants range from hours to days without HFIP and without stirring. The order of fibril formation by wild-type IAPP and the F15 variants is the same in the presence or absence of HFIP (Figure 9 and Table 2). TLe, with the lowest α-helical propensity and highest β-sheet propensity, takes the longest time to form amyloid fibrils, while the Ile variant has a longer lag phase and longer growth phase than the wild type. Variants with unbranched side chains at position 15 form amyloid faster. We also compared the three single aromatic to leucine mutants in the absence of HFIP and found the same rank order as observed in 2% HFIP; F15L formed amyloid more rapidly than the wild type, while both F23L and Y37L did so more slowly than the wild type, with Y37L being the slowest (Table 2). These experiments confirm that the results are not an artifact of solvent composition.

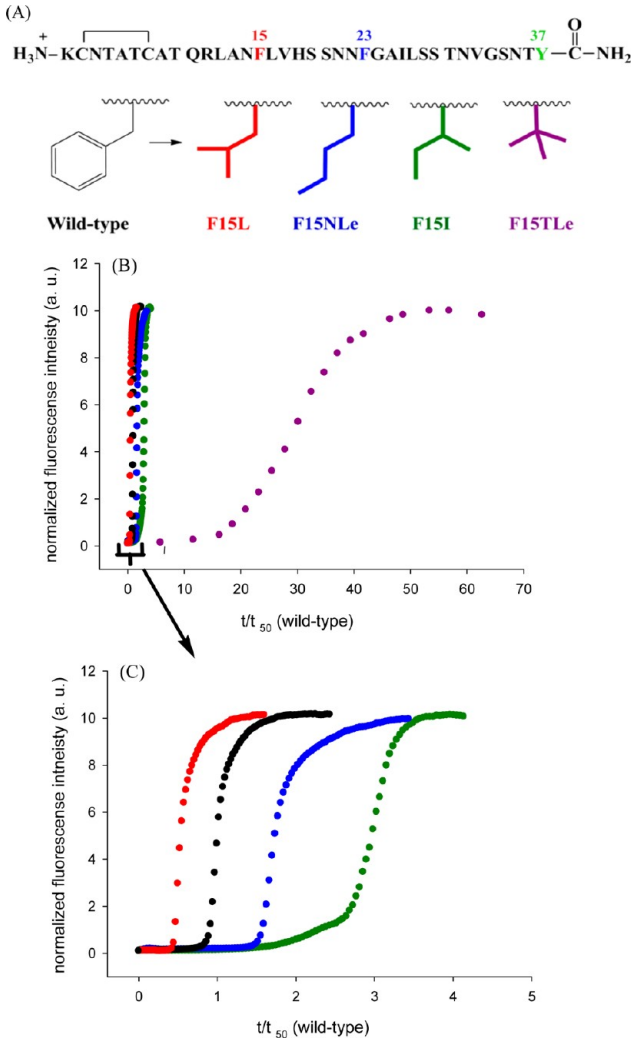

Figure 6. The rate of amyloid formation that is affected by substitution at position 15, but there is no correlation with β-sheet propensity. (A) A series of varients with isomeric four-carbon side chains were analyzed. These "mutations" change α-helix propensity and β-sheet propensity but maintain hydrophobicity. (B) Thioflavin T fluorescence-monitored kinetic experiments: black for wild-type IAPP, red for F15L-IAPP, blue for F15NLe-IAPP, green for F15I-IAPP, and purple for F15TLe-IAPP. (C) Enlarged plot covering the range of t/t_{50} (wild-type) from 0 to 5.

CONCLUSIONS

The data presented here reveal that the three aromatic residues make different contributions to IAPP amyloid assembly kinetics, with the Y37 substitution having the largest effect. Apparent nonadditive effects were observed between F15 and

dx.doi.org/10.1021/bi3014278 | *Biochemistry* 2013, 52, 333−342

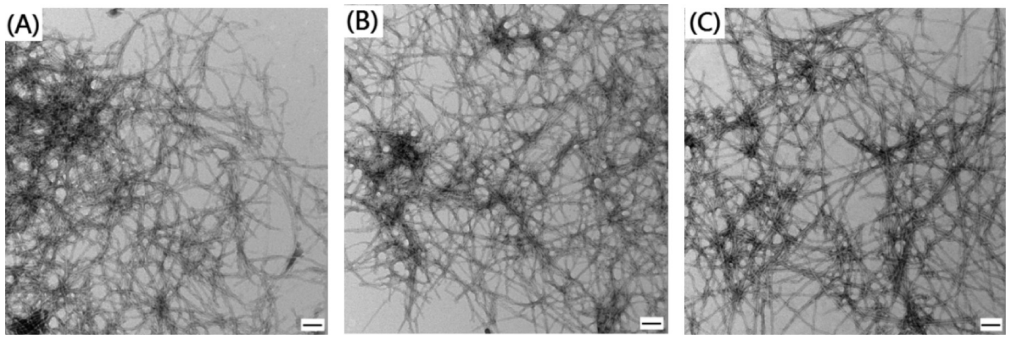

Figure 7. All position 15 variants form amyloid. TEM images recorded at the end of the kinetic runs depicted in Figure 6: (A) F15NLe-IAPP, (B) F15I-IAPP, and (C) F15TLe-IAPP. The scale bar represents 100 nm.

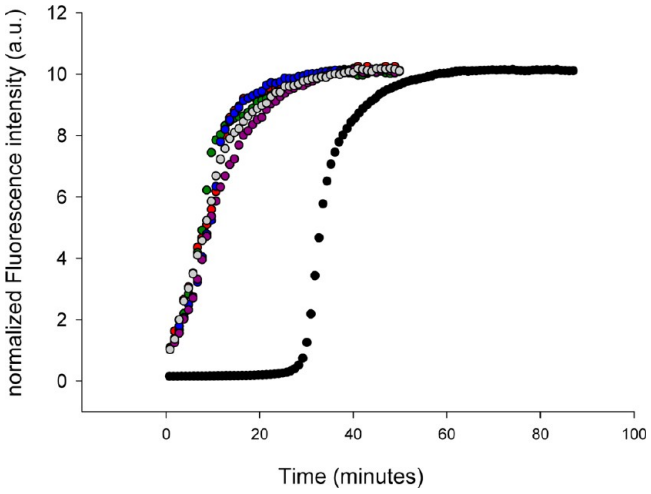

Figure 8. Position 15 variants effectively seed amyloid formation by wild-type IAPP. The results of thioflavin T fluorescence-monitored seeding experiments are shown: black for unseeded wild-type IAPP amyloid formation, gray for wild-type IAPP seeded by wild-type IAPP amyloid fibrils, red for wild-type IAPP seeded by F15L-IAPP amyloid fibrils, blue for wild-type IAPP seeded by F15NLe-IAPP amyloid fibrils, green for wild-type IAPP seeded by F15I-IAPP amyloid fibrils, and purple for wild-type IAPP seeded by F15TLe-IAPP amyloid fibrils.

F23 and between F23 and Y37. The effects should be interpreted with caution because, as noted, amyloid formation is a complex process involving multiple steps and the analysis of nonadditive interactions is less straightforward than analysis of the simple folding of globular proteins. Nontheless, the results are significant, with the strongest effect observed between F15 and F23. F23 is located in a region proposed to be important for the early stages of the development of β-sheet structure,[45] while F15 has been suggested to be involved in early stages of oligomerization. The observation of nonadditivity might reflect synergy between these processes. *p*-Cyanophenylalanine Tyr FRET measurements argue that F23 and Y37 do not make persistent contacts in the lag phase beyond any formed in the dead time of kinetic measurements.[19] Thus, any nonadditive interactions between F23 and Y37 are unlikely to result from long-lived direct contacts formed in the lag phase. It is worth noting that the relative deviation from simple additive behavior is smaller for this pair than for the duo of F15 and F23. The two residues are distant from each other in an individual chain; however, the supermolecular structure of the protofibrils brings F23 in one chain close to Y37 in the adjacent stack of monomers (Figure 1), and this might account for nonadditivity.

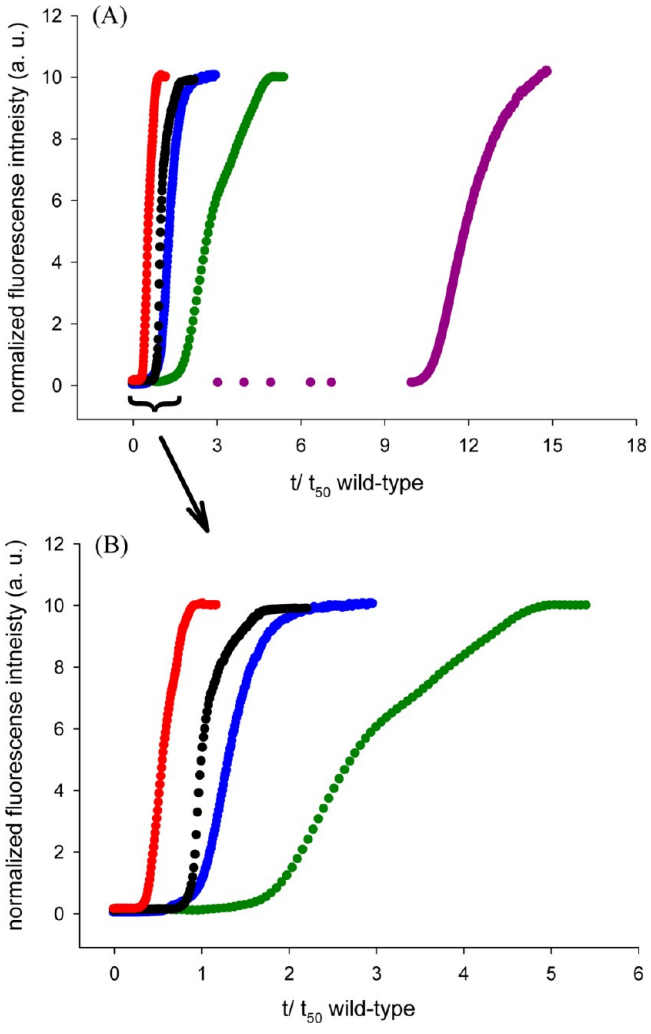

Figure 9. Rank order of amyloid formation by the F15 variants is independent of HFIP. (A) Thioflavin T fluorescence-monitored kinetic experiments in the absence of HFIP without stirring. The final peptide concentration is 16 μM in 20 mM Tris buffer (pH 7.4): black for wild-type IAPP, red for F15L-IAPP, blue for F15NLe-IAPP, green for F15I-IAPP, and purple for F15TLe-IAPP. (B) Enlarged plot covering the range of t/t_{50} (wild-type) from 0 to 6.

The F23C$_\beta$ to Y37C$_\beta$ distances are 12.2 ± 3.5 Å in the NMR-based model of IAPP amyloid.

F15 is within the region proposed to be important for early contact formation during IAPP oligomerization, and several groups have proposed that the initial events involve helix

dx.doi.org/10.1021/bi3014278 | *Biochemistry* 2013, 52, 333−342

Table 2. (A) Kinetic Parameters for Wild-Type IAPP, Single Aromatic to Leu Mutants, and F15 Variants for Amyloid Formation in the Absence of HFIP and (B) Comparison of Kinetic Parameters Normalized with Respect to the Wild Type for Single Aromatic to Leu Mutants and F15 Variants in the Presence and Absence of HFIP[a]

(A)

peptide	wild type	F15L	F23L	Y37L	F15NLe	F15I	F15TLe
lag time (h)	16 ± 1.3[b]	9.8 ± 0.1	38 ± 0.6	42 ± 2.3	20 ± 1.7	41 ± 2.3	267 ± 4
t_{50} (h)	23 ± 0.9	11 ± 0.1	42 ± 1.7	63 ± 2.8	31 ± 1.3	61 ± 5.8	276 ± 6

(B)

parameter	HFIP	F15L	F23L	Y37L	F15NLe	F15I	F15TLe
lag time/wild-type lag time	present	0.4 ± 0.08[c]	1.7 ± 0.4	2.1 ± 0.5	1.9 ± 0.4	2.3 ± 0.5	22 ± 5
t_{50}/wild-type t_{50}	present	0.4 ± 0.08	1.7 ± 0.3	2.8 ± 0.5	1.8 ± 0.4	2.9 ± 0.6	28 ± 6
lag time/wild-type lag time	absent	0.6 ± 0.08	2.4 ± 0.2	2.6 ± 0.3	1.3 ± 0.1	2.6 ± 0.3	17 ± 1.4
t_{50}/wild-type t_{50}	absent	0.5 ± 0.02	1.8 ± 0.1	2.7 ± 0.2	1.3 ± 0.1	2.7 ± 0.3	12 ± 0.5

[a]Experiments were conducted at 25 °C and pH 7.4 in 20 mM Tris-HCl in the presence and absence of HFIP. [b]The quoted uncertainty is the standard deviation. [c]The uncertainty was calculated by standard propagation of error.

formation with the region of residues 8−20 or 8−22.[22,34,35,37] In this model, initial association is driven by the thermodynamic linkage between helix formation and oligomerization. Our analysis of the effect of substitutions at position 15 is broadly consistent with this model because the substitutions with high β-sheet propensity, but low α-helical propensity, have longer lag phases than the wild type. Substitutions with high α-helical propensity and lower β-sheet propensity form amyloid more rapidly with shorter lag phases.

It is interesting to compare these results with a recent study of aromatic residues in the Alzheimer's Aβ peptide.[46] Aβ contains a pair of adjacent Phe residues at positions 19 and 20. The peptide still forms amyloid if both are replaced with Leu or Ile, indicating that aromatic side chains are not required at these sites. These substitutions have the opposite effect in Aβ compared to IAPP; faster amyloid formation was observed for the substitution that increased β-sheet propensity (Ile) compared to the one that lowered β-sheet propensity (Leu). In a separate study, the consequences of a series of substitutions at position −19 were examined in a Aβ−GFP construct.[47] Amyloid formation was found to be dependent on the β-sheet propensity, with a higher β-sheet propensity correlating with enhanced aggregation, although no kinetic data were obtained. Aβ, like IAPP, has been proposed to populate a helical intermediate during amyloid formation in vitro.[48] Within this context, one can still rationalize the effects of F19 mutations and F19 and F20 double mutations; perhaps the helical structure does not include this segment of Aβ, or perhaps helical structure in this portion of the chain introduces new interactions that slow aggregation.

■ ASSOCIATED CONTENT

Supporting Information

A figure showing the primary sequence of IAPP from different species, a figure showing the results of 25 independent kinetic experiments with wild-type IAPP, figures showing more TEM fibril images collected at the end of the kinetic experiments, a figure showing CD spectra collected at the end of the kinetic experiments for the aromatic mutants, a figure showing the effect of varying the pH on the rate of amyloid formation by wild-type human IAPP, figures comparing the kinetic curves for each aromatic mutant to that of wild-type IAPP, a figure showing single aromatic to leucine mutants that were seeded by wild-type fibrils, another CD spectrum collected at the end of the kinetic experiments for the F15 variants, a table giving amino acid side chain parameters, and a table giving kinetic parameters for F15NLe, F15I, and F15Tle in the presence of HFIP. This material is available free of charge via the Internet at http://pubs.acs.org.

■ AUTHOR INFORMATION

Corresponding Author

*Phone: (631) 632-9547. E-mail: daniel.raleigh@stonybrook.edu.

Funding

Sponsored by National Institutes of Health Grant GM078114 to D.P.R.

Notes

The authors declare no competing financial interest.

■ ACKNOWLEDGMENTS

We thank Dr. Peter Marek and Dr. Ping Cao for assistance with experiments and members of the Raleigh group for helpful discussions.

■ ABBREVIATIONS

CD, circular dichroism; F15L-IAPP, Phe-15 to Leu variant of human islet amyloid polypeptide; F15NLe-IAPP, Phe-15 to norleucine variant of human islet amyloid polypeptide; F15I-IAPP, Phe-15 to Ile variant of human islet amyloid polypeptide; F15Tle-IAPP, Phe-15 to *tert*-leucine variant of human islet amyloid polypeptide; F23L-IAPP, Phe-23 to Leu variant of human islet amyloid polypeptide; Y37L-IAPP, Tyr-37 to Leu variant of human islet amyloid polypeptide; F15L/F23L-IAPP, Phe-15 to Leu, Phe-23 to Leu variant of human islet amyloid polypeptide; F15L/Y37L-IAPP, Phe-15 to Leu, Tyr-37 to Leu variant of human islet amyloid polypeptide; F23L/Y37L-IAPP, Phe-23 to Leu, Tyr-37 to Leu variant of human islet amyloid polypeptide; 3XL-IAPP, Phe-15 to Leu, Tyr-37 to Leu, Phe-23 to Leu variant of human islet amyloid polypeptide; IAPP, human islet amyloid polypeptide; NLe, norleucine; TLe, *tert*-leucine (2-amino-3,3-dimethylbutyric acid); t_{50}, time required for 50% of the total signal change in a kinetic experiment; TEM, transmission electron microscopy; t_{lag}, lag time of a kinetic experiment.

■ REFERENCES

(1) Sipe, J. D. (1994) Amyloidosis. *Crit. Rev. Clin. Lab. Sci. 31*, 325−354.

(2) Selkoe, D. J. (2004) Cell biology of protein misfolding: The examples of Alzheimer's and Parkinson's diseases. *Nat. Cell Biol. 6*, 1054−1061.
(3) Chiti, F., and Dobson, C. M. (2006) Protein misfolding, functional amyloid, and human disease. *Annu. Rev. Biochem. 75*, 333−366.
(4) Lansbury, P. T., and Lashuel, H. A. (2006) A century-old debate on protein aggregation and neurodegeneration enters the clinic. *Nature 443*, 774−779.
(5) Mitraki, A. (2010) Protein aggregation: From inclusion bodies to amyloid and biomaterials. *Adv. Protein Chem. Struct. Biol. 79*, 89−125.
(6) Westermark, P., Wernstedt, C., Wilander, E., Hayden, D. W., Obrien, T. D., and Johnson, K. H. (1987) Amyloid fibrils in human insulinoma and islets of langerhans of the diabetic cat are derived from a neuropeptide-like protein also present in normal islet cells. *Proc. Natl. Acad. Sci. U.S.A. 84*, 3881−3885.
(7) Clark, A., Lewis, C. E., Willis, A. C., Cooper, G. J. S., Morris, J. F., Reid, K. B. M., and Turner, R. C. (1987) Islet amyloid formed from diabetes-associated prptide may be pathogenic in type-2 diabetes. *Lancet 2*, 231−234.
(8) Westermark, P., Andersson, A., and Westermark, G. T. (2011) Islet amyloid polypeptide, islet amyloid, and diabetes mellitus. *Physiol. Rev. 91*, 795−826.
(9) Hutton, J. C. (1989) The insulin secretory granule. *Diabetologia 32*, 271−281.
(10) Kahn, S. E., Dalessio, D. A., Schwartz, M. W., Fujimoto, W. Y., Ensinck, J. W., Taborsky, G. J., and Porte, D. (1990) Evidence of cosecretion of islet amyloid polypeptide and insulin by β-cells. *Diabetes 39*, 634−638.
(11) Nishi, M., Sanke, T., Nagamatsu, S., Bell, G. I., and Steiner, D. F. (1990) Islet amyloid polypeptide: A new β-cell secretory product related islet amyloid deposits. *J. Biol. Chem. 265*, 4173−4176.
(12) Westermark, G. T., Westermark, P., Berne, C., Korsgren, O., and Nordic Network Clin Islet, T. (2008) Widespread amyloid deposition in transplanted human pancreatic islets. *N. Engl. J. Med. 359*, 977−979.
(13) Westermark, G. T., Westermark, P., Nordin, A., Tornelius, E., and Andersson, A. (2003) Formation of amyloid in human pancreatic islets transplanted to the liver and spleen of nude mice. *Upsala J. Med. Sci. 108*, 193−203.
(14) Potter, K. J., Abedini, A., Marek, P., Klimek, A. M., Butterworth, S., Driscoll, M., Baker, R., Nilsson, M. R., Warnock, G. L., Oberholzer, J., Bertera, S., Trucco, M., Korbutt, G. S., Fraser, P. E., Raleigh, D. P., and Verchere, C. B. (2010) Islet amyloid deposition limits the viability of human islet grafts but not porcine islet grafts. *Proc. Natl. Acad. Sci. U.S.A. 107*, 4305−4310.
(15) Gazit, E. (2002) A possible role for π-stacking in the self-assembly of amyloid fibrils. *FEBS J. 16*, 77−83.
(16) Marek, P., Abedini, A., Song, B. B., Kanungo, M., Johnson, M. E., Gupta, R., Zaman, W., Wong, S. S., and Raleigh, D. P. (2007) Aromatic interactions are not required for amyloid fibril formation by islet amyloid polypeptide but do influence the rate of fibril formation and fibril morphology. *Biochemistry 46*, 3255−3261.
(17) Tracz, S. M., Abedini, A., Driscoll, M., and Raleigh, D. P. (2004) Role of aromatic interactions in amyloid formation by peptides derived from human amylin. *Biochemistry 43*, 15901−15908.
(18) Padrick, S. B., and Miranker, A. D. (2001) Islet amyloid polypeptide: Identification of long-range contacts and local order on the fibrillogenesis pathway. *J. Mol. Biol. 308*, 783−794.
(19) Marek, P., Mukherjee, S., Zanni, M. T., and Raleigh, D. P. (2010) Residue-specific, real-time characterization of lag-phase species and fibril growth during amyloid formation: A combined fluorescence and IR study of p-cyanophenylalanine analogs of islet amyloid polypeptide. *J. Mol. Biol. 400*, 878−888.
(20) Lorenzo, A., Razzaboni, B., Weir, G. C., and Yankner, B. A. (1994) Pancreatic-islet cell toxicity of amylin associated with type-2 diabetes mellitus. *Nature 368*, 756−760.
(21) Butler, A. E., Janson, J., Bonner-Weir, S., Ritzel, R., Rizza, R. A., and Butler, P. C. (2003) β-Cell deficit and increased β-cell apoptosis in humans with type 2 diabetes. *Diabetes 52*, 102−110.
(22) Wiltzius, J. J. W., Sievers, S. A., Sawaya, M. R., and Eisenberg, D. (2009) Atomic structures of IAPP (amylin) fusions suggest a mechanism for fibrillation and the role of insulin in the process. *Protein Sci. 18*, 1521−1530.
(23) Abedini, A., and Raleigh, D. P. (2005) Incorporation of pseudoproline derivatives allows the facile synthesis of human IAPP, a highly amyloidogenic and aggregation-prone polypeptide. *Org. Lett. 7*, 693−696.
(24) Tam, J. P., Wu, C. R., Liu, W., and Zhang, J. W. (1991) Disulfide bond formation in peptides by dimethyl-sulfoxide: Scope and applications. *J. Am. Chem. Soc. 113*, 6657−6662.
(25) Abedini, A., Singh, G., and Raleigh, D. P. (2006) Recovery and purification of highly aggregation-prone disulfide-containing peptides: Application to islet amyloid polypeptide. *Anal. Biochem. 351*, 181−186.
(26) Luca, S., Yau, W. M., Leapman, R., and Tycko, R. (2007) Peptide conformation and supramolecular organization in amylin fibrils: Constraints from solid-state NMR. *Biochemistry 46*, 13505−13522.
(27) Levine, H. (1993) Thioflavine-T interaction with synthetic Alzheimers-disease β-amyloid peptides: Detection of amyloid aggregation in solution. *Protein Sci. 2*, 404−410.
(28) Padrick, S. B., and Miranker, A. D. (2002) Islet amyloid: Phase partitioning and secondary nucleation are central to the mechanism of fibrillogenesis. *Biochemistry 41*, 4694−4703.
(29) Abedini, A., and Raleigh, D. P. (2005) The role of His-18 in amyloid formation by human islet amyloid polypeptide. *Biochemistry 44*, 16284−16291.
(30) O'Nuallain, B., Williams, A. D., Westermark, P., and Wetzel, R. (2004) Seeding specificity in amyloid growth induced by heterologous fibrils. *J. Biol. Chem. 279*, 17490−17499.
(31) Krebs, M. R. H., Morozova-Roche, L. A., Daniel, K., Robinson, C. V., and Dobson, C. M. (2004) Observation of sequence specificity in the seeding of protein amyloid fibrils. *Protein Sci. 13*, 1933−1938.
(32) Williamson, J. A., and Miranker, A. D. (2007) Direct detection of transient α-helical states in islet amyloid polypeptide. *Protein Sci. 16*, 110−117.
(33) Nanga, R. P. R., Brender, J. R., Xu, J. D., Hartman, K., Subramanian, V., and Ramamoorthy, A. (2009) Three-dimensional structure and orientation of rat islet amyloid polypeptide protein in a membrane environment by solution NMR spectroscopy. *J. Am. Chem. Soc. 131*, 8252−8261.
(34) Abedini, A., and Raleigh, D. P. (2009) A critical assessment of the role of helical intermediates in amyloid formation by natively unfolded proteins and polypeptides. *Protein Eng., Des. Sel. 22*, 453−459.
(35) Abedini, A., and Raleigh, D. P. (2009) A role for helical intermediates in amyloid formation by natively unfolded polypeptides? *Phys. Biol. 6*, 15005.
(36) Cao, P., Meng, F., Abedini, A., and Raleigh, D. P. (2010) The ability of rodent islet amyloid polypeptide to inhibit amyloid formation by human islet amyloid polypeptide has important implications for the mechanism of amyloid formation and the design of inhibitors. *Biochemistry 49*, 872−881.
(37) Williamson, J. A., Loria, J. P., and Miranker, A. D. (2009) Helix stabilization precedes aqueous and bilayer-catalyzed fiber formation in islet amyloid polypeptide. *J. Mol. Biol. 393*, 383−396.
(38) Gilead, S., Wolfenson, H., and Gazit, E. (2006) Molecular mapping of the recognition interface between the islet amyloid polypeptide and insulin. *Angew. Chem., Int. Ed. 45*, 6476−6480.
(39) Fauchere, J. L., Charton, M., Kier, L. B., Verloop, A., and Pliska, V. (1988) Amino acid side chain parameters for correlation studies in biology and pharmacology. *Int. J. Pept. Protein Res. 32*, 269−278.
(40) Paterson, Y., and Leach, S. J. (1978) Effect of side-chain branching on theoretically predicted conformational space available to amino-acid-residues. *Macromolecules 11*, 409−415.
(41) Minor, D. L., and Kim, P. S. (1994) Measurement of the β-sheet-forming propensities of amino acids. *Nature 367*, 660−663.
(42) Street, A. G., and Mayo, S. L. (1999) Intrinsic β-sheet propensities result from van der Waals interactions between side

chains and the local backbone. *Proc. Natl. Acad. Sci. U.S.A. 96*, 9074−9076.
(43) Wiltzius, J. J., Sievers, S. A., Sawaya, M. R., Cascio, D., Popov, D., Riekel, C., and Eisenberg, D. (2008) Atomic structure of the cross-β spine of islet amyloid polypeptide (amylin). *Protein Sci. 17*, 1467−1474.
(44) Lyu, P. C., Sherman, J. C., Chen, A., and Kallenbach, N. R. (1991) α-Helix stabilization by natural and unnatural amino-acids with alkyl side-chains. *Proc. Natl. Acad. Sci. U.S.A. 88*, 5317−5320.
(45) Shim, S. H., Gupta, R., Ling, Y. L., Strasfeld, D. B., Raleigh, D. P., and Zanni, M. T. (2009) Two-dimensional IR spectroscopy and isotope labeling defines the pathway of amyloid formation with residue-specific resolution. *Proc. Natl. Acad. Sci. U.S.A. 106*, 6614−6619.
(46) Armstrong, A. H., Chen, J., McKoy, A. F., and Hecht, M. H. (2011) Mutations that replace aromatic side chains promote aggregation of the Alzheimer's Aβ peptide. *Biochemistry 50*, 4058−4067.
(47) de Groot, N. S., Aviles, F. X., Vendrell, J., and Ventura, S. (2006) Mutagenesis of the central hydrophobic cluster in Aβ42 Alzheimer's pepticle: Side-chain properties correlate with aggregation propensities. *FEBS J. 273*, 658−668.
(48) Kirkitadze, M. D., Condron, M. M., and Teplow, D. B. (2001) Identification and characterization of key kinetic intermediates in amyloid β-protein fibrillogenesis. *J. Mol. Biol. 312*, 1103−1119.